Silicon Vacancy (SiV⁻) Nanodiamonds as High Performance Near Infrared Emitters for Live Cell Imaging and Particle Tracking

Weina Liu,[†,∇,‡] Yan Liu,[§,‡] Viatcheslav N. Agafonov,[⊥] Haoyuan Qi,[∥] Kaloian Koynov,[†] Valery A. Davydov,[#] Rustem Uzbekov,[○,+] Ute Kaiser,[∥] Theo Lasser,[†] Fedor Jelezko,[§,] Tanja Weil[†,∇,*]*

†Max-Planck-Institute for Polymer Research, Ackermannweg 10, 55128 Mainz, Germany

∇Institute of Inorganic Chemistry I, Ulm University, Albert-Einstein-Allee 11, 89081 Ulm, Germany

§Institute for Quantum Optics, Ulm University, Albert-Einstein-Allee 11, 89081 Ulm, Germany

⊥GREMAN, UMR CNRS-7347, Université de Tours, 37200, Tours, France

∥Central Facility for Electron Microscopy, Ulm University, Albert-Einstein-Allee 11, 89081 Ulm, Germany

#L.F. Vereshchagin Institute for High Pressure Physics, The Russian Academy of Sciences, Troitsk, Moscow, 108840, Russia

○Laboratoire Biologie Cellulaire et Microscopie Electronique, Faculté de Médecine, Université François Rabelais, 37032 Tours, France

+Faculty of Bioengineering and Bioinformatics, Moscow State University, 119992, Leninskye gory 73, Moscow, Russia.

KEYWORDS: Nanodiamond, silicon vacancy color center, SiV$^-$, near infrared cellular imaging, live cell particle tracking.

ABSTRACT Using tailored nanodiamonds with negatively charged silicon-vacancy (SiV$^-$) color centers we performed a series of intracellular experiments. These nanodiamonds with SiV$^-$ centers (NDs-SiV$^-$) were obtained by high-pressure high-temperature (HPHT) synthesis based on metal catalysts-free hydrocarbon HPHT growth. They were coated by a polypeptide biopolymer allowing efficient cellular uptake. High photostability and narrow emission in the near infrared region allows tracking of functionalized NDs-SiV$^-$ in living cells. The excellent optical properties render NDs-SiV$^-$ promising nanoemitters for various bioimaging applications. Furthermore, cellular tracking with detailed time, spatial, and spectral information paves the way to intracellular thermometry based on NDs-SiV$^-$.

Nanodiamonds (NDs) with color centers have emerged as high performance emitters for advanced bioimaging and sensing applications such as super-resolution live-cell imaging and nanoscale magnetic resonance providing high spatial resolution and sensitivity down to the single particle level.[1-4] Until recently, most biological applications of NDs were based on their nitrogen-vacancy (NDs-NVs) color centers. These ND-NVs are commercially available and can be produced in different sizes and with varying numbers of NVs.[5] Their optical properties have been intensively studied, including its neutral (NV^0) and charged (NV$^-$) forms. The NV$^-$ has a triplet structure of electron spin states and has been widely applied for e.g. optical detection of electric and magnetic fields or temperature sensing. [6-8] However, both zero phonon lines (ZPLs) of NV^0 and NV$^-$ are accompanied by broad phonon sidebands, leading to broad fluorescence emission spanning from ~550 nm to 800 nm.[7] Thus, their fluorescence spectrum partly overlaps with any backround and dual/multi-color imaging becomes more challenging.

In contrast, NDs with negatively charged silicon vacancy (SiV⁻) centers have recently received considerable attention as potential high performance bioimaging probes due to their attractive optical properties that show distinct differences to the NV⁻ center. In the ND crystal lattice, the Si atom with its larger size compared to carbon replaces two carbon atoms, and it is located between these two vacancies (a fragment of the structure with silicon (Si) is shown in Fig.1b). As a result, the Si atom is surrounded by 6 carbon atoms in the diamond crystal of the same distance of around 1.94 Å. The site occupied by Si conserves the inversion center resulting in a low sensitivity to strain and contributes to a narrowing of the optical emission.[9] Due to the low electron-phonon coupling, more than 70% of SiV⁻ fluorescence is dominated by its sharp zero-phonon line (ZPL).[10] As a result, the photoluminescence (PL) spectra of SiV⁻ centers in NDs consist of a dominant and narrow ZPL at ~738 nm with full width at half maximum (FWHM) of approximately 4 nm, and a weak phonon sideband at ~760 nm.[10] In this way, the sharp emission band of SiV⁻ containing nanodiamonds (ND-SiV⁻) is in the near infrared (NIR) range (>700 nm) allowing a deeper tissue penetration an important feature for *in vivo* optical imaging.[11-12] Moreover, the peak position of the ZPL of SiV⁻ has a temprature signature, which is linearly correlated to temperature changes in the range of 295 ± 5K with sub-kelvin sensitivity.[13] The combination of NIR emission, narrow bandwidth, high (photo) chemical stability, and temperature dependent ZPL[14-15] renders ND-SiV⁻ promising candidates for imaging and sensing applications in lifesciences and biology such as super-resolution bioimaging and nano thermometry.

Early reports on NDs-SiV⁻ were based on high-pressure high-temperature (HPHT) synthesis in the presence of transition metal catalysts followed by ion implantation or chemical vapour deposition (CVD) growth.[16-18] But the synthesis of NDs with different color centers can be also realized by the metal catalists-free variant of HPHT method based on the conversion of organic and heteroorganic solids (polycyclic aromatic hydrocarbons) into diamond.[19] Previously, the

NDs with different color centers have been synthesized by metal catalysts-free mixtures of hydro- and fluorocarbons and molecules containing the desired dopants.[20] In this way, no cytotoxic metal catalysts were applied that could remain in the NDs. This method further allowed controlling ND sizes as well as the concentration of the color centers by adjusting the composition of reagents, pressure, temperature and temporal processing.[21-22]

The use of NDs in biology makes it necessary to introduce surface coatings to enhance their colloidal stability in aqueous media as well as to introduce binding ligands to facilitate specific interactions of NDs with their imaging or sensing targets.[23] Therefore, several surface modification strategies have been reported such as controlled polymerization from NDs, complexation of already prefunctionalized polymers, as well as ND coating by a dense polydopamine and lipid shell.[24-26] For sensing applications, the introduction of thin layer coatings is another critical parameter to minimize the distance between color centers and the sensing targets in their surrounding. Meanwhile, the fast developing field of super-resolution microscopy has overcome the resolution limitations for NDs in bioimaging and biosensing applications, and the correlated imaging tools provide comprehensive information to evaluate the bioactivities of the NDs in biosystems.[1, 27]

Here we report an optimized HPHT approach that allows the preparation of NDs-SiV$^-$ with radii of about 50 nm and without the presence of NV$^-$ centers. The ND-SiV$^-$ surface was coated by a protein-derived biopolymer based on multiple electrostatic interactions and NDs-SiV$^-$ nanoemitters with enhanced colloidal stability were obtained. These coated NDs-SiV$^-$ show a good uptake by Hela cells based on an endocytosis mechanism. For the first time, NDs-SiV$^-$ were imaged inside living cells based on their NIR emission, high photostability and sharp ZPL. The ND-SiV$^-$ also allowed long-time lapse cellular tracking without photo-bleaching or blinking during the observation time. Therefore, we performed preliminary tracking

experiments attempting to monitor the mobility of NDs-SiV⁻, their ZPL spectra and fluorescence intensity of the SiV centers inside living cells. We therefore state, that these NDs-SiV⁻ are usefull as biocompatibe NIR emitters for cell and tissue imaging providing access to local parameters such as temperature gradients. In this way, deeper insights into various biological processes could be obtained where temperature changes may play an important role.

NDs-SiV⁻ HPHT synthesis and surface oxidization. ND-SiV⁻ were obtained by HPHT treatment of the metal catalysts-free growth system based on a homogeneous mixture of naphthalene ($C_{10}H_8$, Chemapol), octafluoronaphthalene ($C_{10}F_8$, Alfa Aesar), ultra-small NDs (3-4 nm, SkySpring) and tetrakis(trimethylsilyl)silane ($C_{12}H_{36}Si_5$, Stream Chemicals Co.), which was used as the doping component (Fig. 1a). Introduction of fluorine-containing compounds into the growth system leads to the reduction of the content of NV centers in NDs-SiV⁻.[20-21, 28] Although self-nucleation of NDs can occur under HPHT conditions, seeded growth provides ND particles in higher yields. Therefore, detonation NDs of 3 to 5 nm were introduced into growth medium that serve as seeds in the HPHT reaction. The carbon and silicon source mixture, naphthalene/octafluoronaphthalene/detonation NDs and tetrakis(trimethylsilyl)silane, respectively, were cold-pressed as a tablet (5 mm diameter and 4 mm height), and the tablet was placed into a graphite container, which simultaneously served as a heater for the high-pressure Toroid-type apparatus. The HPHT procedure consisted of the following steps: (1) loading the apparatus to high-pressure (8.0 GPa) at room temperature, (2) heating the apparatus to high-temperature (~1400°C) for diamond formation, and (3) an isothermal exposure for short time (3 s) at the same temperature. The resulting high-pressure status was quenched to room temperature, while still maintaining high pressure. Five batches were synthesized under the same conditions of T (temperature), P (pressure), and t (reaction time) and combined to maximize the amount of powder. Subsequently, steel ball milling was applied to break the diamonds into nanometre-sized ND particles. A primary acid cleaning step with oxidizing acids

such as $HNO_3/HClO_4/H_2SO_4$ at 230 °C for 5 h generated a powder, which was then neutralized with NH_4OH buffer, washed again and dried as depicted in Fig. 1a.

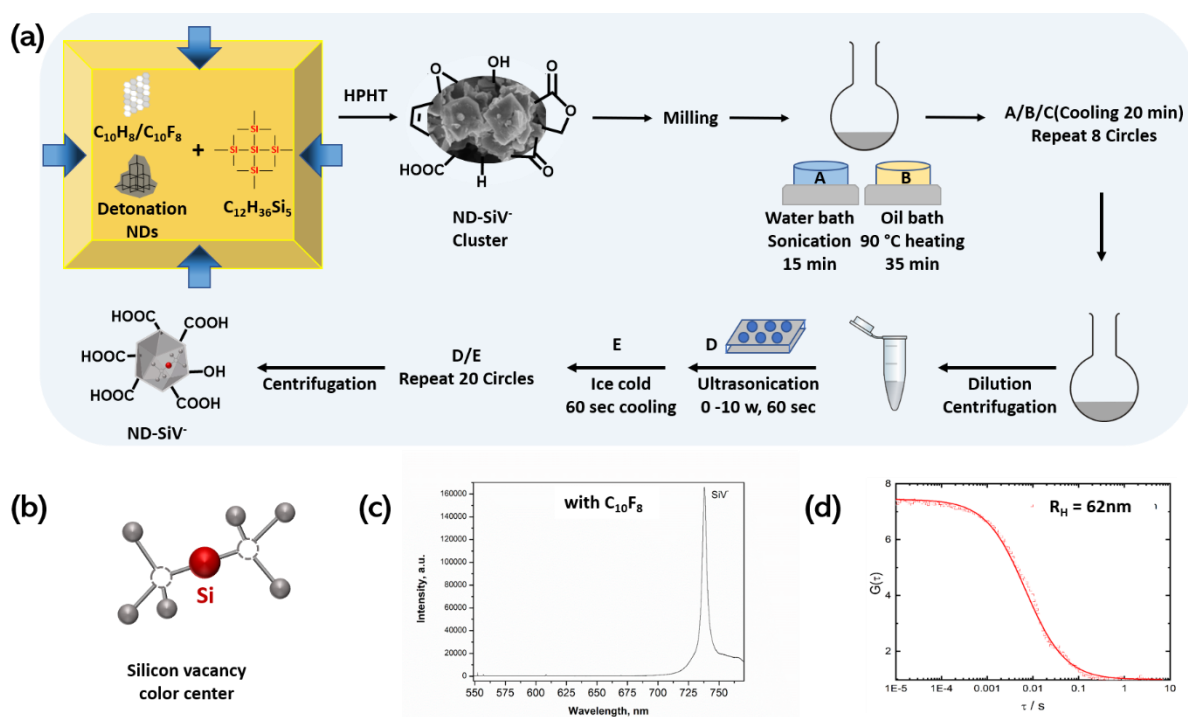Figure 1. (a) Scheme of ND-SiV⁻ HPHT synthesis with $C_{10}H_8/C_{10}F_8$ and detonation NDs as carbon source and silane $C_{12}H_{36}Si_5$ as silicon source. Raw ND-SiV⁻ clusters were obtained and imaged by scanning electron microscopy (SEM, with full SEM image in Fig. S2). The following milling, acid cleaning, sonication, and ultrasonication steps (A-E) are also showed in (a). (b) Atomic structure of silicon vancancy color center. (c) Photoluminance spectra of HPHT NDs-SiV⁻ synthesized with $C_{10}F_8$. (d) Fluorescence correlation spectroscopy autocorrelation curve of NDs-SiV⁻.

Surface cleaning and oxidization with strong acid treatment combined with sonication and powerfull ultrasonication (Fig. 1a, with experimental detail in supporting information) was crucial to generate discrete and stable ND suspensions in water with polar carboxylic acid surface groups that reveal stable fluorescence[29] and for further chemical modifications.[30] Briefly, NDs-SiV⁻ raw material (25 mg) was dispersed in a concentrated acid mixture of HNO_3-H_2SO_4-$HClO_4$ (6 ml, volume ratio1:1:1) and refluxed at 90 °C for 8 hours. After each 35 mins of reflux, NDs-SiV⁻/acid mixture were cooled down to room temperature and treated by water

6

bath sonication, which was applied to dissociate NDs-SiV$^-$ from their aggregates, and to improve the exposure of different facets of the NDs-SiV$^-$ to the oxidizing acid mixture. Thereafter, NDs-SiV$^-$ were washed by centrifugation to remove the acid in the supernatant, resuspended in MilliQ water, and treated by ultrasonication to further separate the clustered NDs-SiV$^-$. The entire process of sonication combined with acid treatment, as well as the subsequent ultrasonication (step A-E, Fig. 1a) was repeated three times as described in detail in the supporting information. Finally, the NDs-SiV$^-$ were re-suspend in water and all non-suspended NDs were removed by low speed centrifugation (885 $\times$g, 10 mins).

This approach yielded about 5 mg of NDs-SiV$^-$ that formed a stable water suspension providing polar surface groups suitable for further studies. The NDs-SiV$^-$ exhibited negative zeta-potential with single peak distribution (ζ = −29.33 mv, Fig. 2g), and an even size distribution (radius = 52.3 $\pm$ 3.6 nm, Fig. 2f) with a polydispersity index (PDI) value of 0.16 according to dynamic according to light scattering measurement. The average hydrodynamic radius of fluoresencent NDs-SiV$^-$ of 62 $\pm$ 5 nm (Fig. 1d) was determined by Fluorescence Correlation Spectroscopy (FCS)[31] in aqueous solution. The small difference in size compared to DLS could be attributed to the differences in polydispersity averaging index of FCS and DLS measurements.[32]

Scanning and transmission electron microscopy (SEM and TEM, Fig. S2 and S3) showed the formation of diamonds with nano- and micron-size and cuboctahedral shape. The photoluminescence properties of the produced NDs were characterized at ambient conditions by optical spectroscopy. Interestingly, we only observed a very sharp and clear photoluminance spectrum of NDs-SiV$^-$ if $C_{10}F_8$ was applied as starting material (Fig. 1c). In contrast, HPHT synthesis of NDs-SiV$^-$ without $C_{10}F_8$ yielded a mixture of NDs with strong NV$^-$ and SiV$^-$ emission in their photoluminance spectra (Fig. S1). In comparison to NDs-SiV$^-$ synthesised by

chemical vapour deposition (CVD) on a silicon or metal substrate, or silicon implantation of NDs,[33-34] the HPHT ND-SiV$^-$ synthesis reported herein offers several distinct advantages: (1) No metal catalyst is employed that could remain in the NDs as impurity, (2) no post-processing of irradiation or annealing is required to activate the colour centres and (3) the method is scalable up to several milligram quantities, which would allow extensive cell studies with the same batch.

Biopolymer coated NDs-SiV$^-$. The application of NDs-SiV$^-$ for cellular studies requires surface coating that imparts colloidal stability in cell media and allows cellular uptake *via* endocytosis and trafficking to cellular compartments as well as low cellular toxicity. We have previously reported the conversion of proteins into biocompatible NDs surface coatings that have been applied *in vitro* and *in vivo*.[26] Briefly, as shown in Scheme S1, the synthesis was based on the abundant serum protein HSA (human serum albumin) that was chemically modified by reacting ethylenediamine groups with the carboxylic acid surface groups of aspartic acid and glutamic acid residues yielding cationic HSA (cHSA, cationazation).[35-36] cHSA with multiple additional amino groups provides multiple positive net charges required for the subsequent formation of stable complexes with negatively charged NDs-SiV by electrostatic interactions. Then, hydrophilic PEG chains (molecule weight 2000 Da) were conjugated to cHSA to improve the colloidal stability of the modified protein polymer as well as coated NDs-SiV$^-$ (cHSA-PEO, PEGlytion). Next, the polypeptide backbone of cHSA-PEO was unfolded by reduction of the disulfide bridges. The generated free sulfurhydryl groups were capped with *N*-(2-aminoethyl)maleimide to obtain the stable single chain biopolymer (dcHSA-PEO, denaturation). The synthesis and characterization of the biopolymer dcHSA-PEO has been reported previously[26] and is included in the SI (Fig. S8 and Fig. S9).

NDs-SiV$^-$ diluted in boric acid buffer (0.05 mg/mL, 20 mL, pH = 8.4) were mixed with dcHSA-PEO (0.2 mg/mL, 20 mL) *via* titration addition, and coating proceeded through electrostatic absorption overnight. After ultrafiltration (cutoff 30 KD) and centrifugation(17 000g, 30 min × 3), the ND mixture was concentrated and unbound dcHSA-PEO biopolymer was removed. About 1 mg (50% yield) coated NDs-SiV$^-$ were obtained, termed ND$_{SiV}$-polymer. Fig. 2b shows the aberration-corrected high-resolution TEM (AC-HRTEM) image of ND$_{SiV}$-polymer in [0$\bar{1}$1] projection. The ND$_{SiV}$-polymer particles were highly crystalline exhibiting sharp edges along the main crystallographic orientations. In the magnified image (Fig. 2c), the (111) and (022) lattice planes of diamond were clearly resovled. Residual amounts of armophous and non-diamond nanoparticles were also observed *via* AC-HRTEM (Fig. S4), which could not be removed by the acid processing. However, the X-ray diffraction patterns (XRD) of the NDs-SiV$^-$ raw material clearly indicates the typical diamond spectrum with reflections at (111) and (220) that were rather enlarged, and only a low reflection of residual traces of amorphous carbon (Fig. S5).

A uniform and discrete distribution of ND$_{SiV}$-polymer was observed by transmission electron microscopy (TEM, Fig. 2d), with an average radius of 31.6 nm (histogram in Fig. 2e) by analyzing 108 NDs in the TEM image. After polymer encapsulation, ND$_{SiV}$-polymer revealed a hydrodynamic radius of about 63.6 ± 5.3 nm (PDI = 0.1) corresponding to an increase of about 11 nm due to the polymer shell. The ND$_{SiV}$-polymer appeared colloidally stable also in phosphate-buffered saline buffer (PBS, pH = 7.4) and DLS studies only measured a slight increase in the radius of 70 nm with PDI = 0.08. The surface charges of ND$_{SiV}$-polymer appeared positive (ζ = 21.3 mv) due to the presence of the polycationic biopolymer dcHSA-PEO. Nanoparticle surface coatings with positive net charges have been considered beneficial

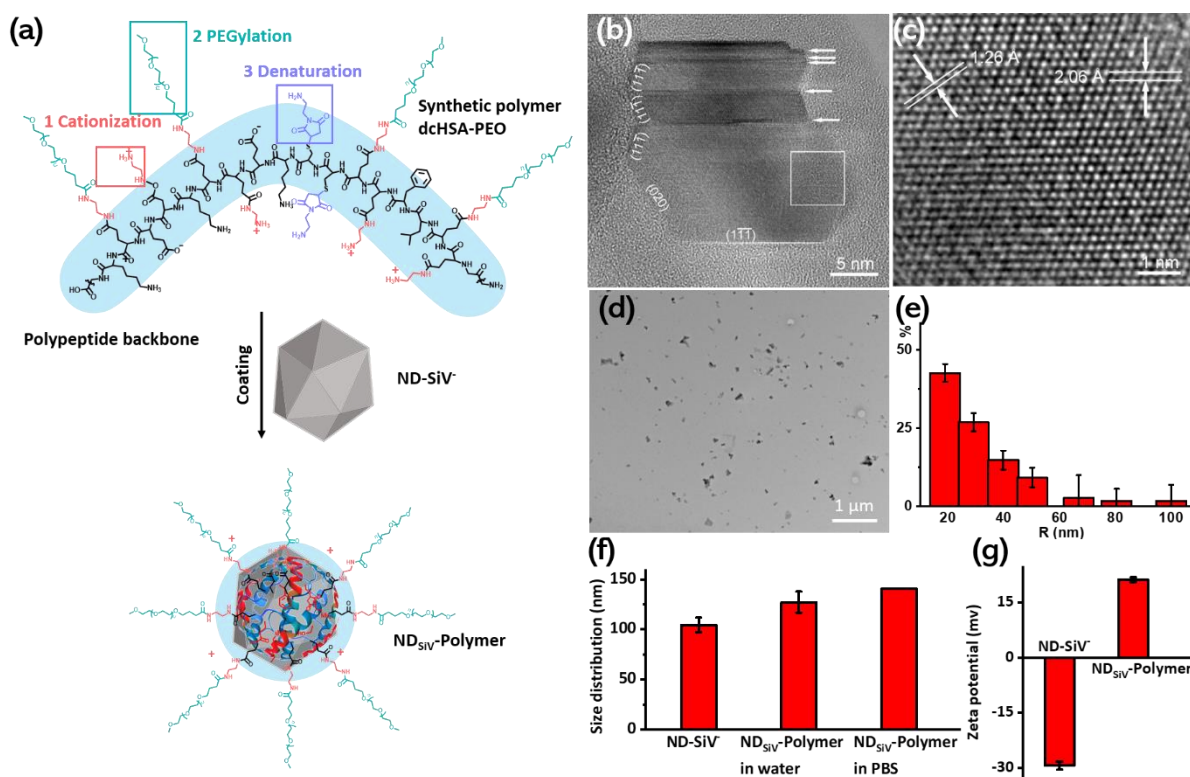to facilitate cellular uptake through interactions with negatively charged cell membranes (Fig. 2f and g).[26, 35]

Figure 2. ND$_{SiV}$-polymer preparation and characterization. (a) NDs-SiV$^-$ modification by the biopolymer dcHSA-PEO coating. (b) [0$\bar{1}$1] AC-HRTEM image of NDs-SiV$^-$ consisting of crystalline domains separated by twin boundaries (marked by arrows). (c) Magnified image from the boxed region in (b), showing the **d**istances between the lattice planes of diamond: *(111) (**d**=2.06 Å) and (022) (**d**=1.26 Å)*. (d)Transmission electron microscopy image of coated NDSiV-polymer. Small cluster can be observed from the TEM images, but most of the NDs are discrete nanoparticles. (e) Histogram of NDs redius, qunatification of 108 NDs from (d). (f) Dynamic light scattering radius of NDs-SiV$^-$ in water and ND$_{SiV}$-polymer in water and PBS buffer. (g) Zeta-potential of NDs-SiV$^-$ and ND$_{SiV}$-polymer.

Live cell imaging of ND$_{SiV}$-polymer. The ND$_{SiV}$-polymer were applied for live cell imaging in Hela cells used as model cell line. ND$_{SiV}$-polymer (0.02 mg/mL) were incubated for 24 h to enable cellular uptake, and efficient cellular uptake into Hela cells was recorded by confocal laser scanning microscopy (CLSM). In a previous study, NDs-SiV$^-$ powder prepared by the

CVD method was directly incubated with cells[33] without stabilizing surface modifications, and only cell membrane labeling was observed after several days of incubation. In our case, ND_{SiV}-polymer were homogeneously distributed inside of the cell (Fig. 3a). In addition due to the high index of refraction, these ND_{SiV}-polymer act as strong light scatterers allowing to distinguish NDs from background fluorescence of Hela cells, which proved to be very helpful for further multiple stained bioimaging. According to Fig. 3a, the images taken in the reflection mode of ND_{SiV}-polymer showed a good localisation match with the ND_{SiV}-polymer fluorescence images (colocolisation coefficient 0.6), indicating most of NDs contained SiV color centers. The nonoverlapping portion was attributed to a small fraction of NDs lacking SiV color centers, since the reflection imaging depicts all NDs particles, and emission imaging only image ND with color centers. However, until now, the mechanism responsible for blinking and bleaching of NDs-SiV$^-$ has not yet been fully investigated.[37] Furthermore, time series scan was processed to evaluate the photostability of ND_{SiV}-polymer. Some of the fluorescent spots bleached after three scanning sweeps (Fig. S13a), but the remaining emitters revealed high stability (Fig. S13b) suitable for cellular imaging and following cellular tracking.

Hela cells incubated with ND_{SiV}-polymer were placed under a customized scanning confocal fluorescence microscope for cell imaging and to subsequently asses single particle tracking (Fig. 3b). The cell culture medium was replaced with PBS buffer to avoid autofluorescence. An excitation laser power of 200 μW (measured before the objective) at 532 nm was used during the confocal scanning experiment. In order to show the outline of the cell which has a relatively low autofluorescence, the maximum photon intensity scale was restrained to 140 kc/s (thousand photon counts per second).

ZPLs of the ND_{SiV}-polymer inside cells were captured with the combined spectrometer, which showed a typical SiV$^-$ spectrum centered around 738 nm and no extra emission in the range of

560 – 837 nm (Fig. 3c). Remarkably, no emission associated to NV centers was detected, which clearly proved the successful reduction of nitrogen in NDs-SiV⁻ by our preparation techniuque ($C_{10}F_8$ during HPHT synthesis). In contrast to bioimaging by NDs-NVs with broad-band emission envelopes that overlap with many dyes and drugs, intense and sharp near infrared ZPL emission of NDs-SiV⁻ were detected, which offer promising features for cellular imaging.
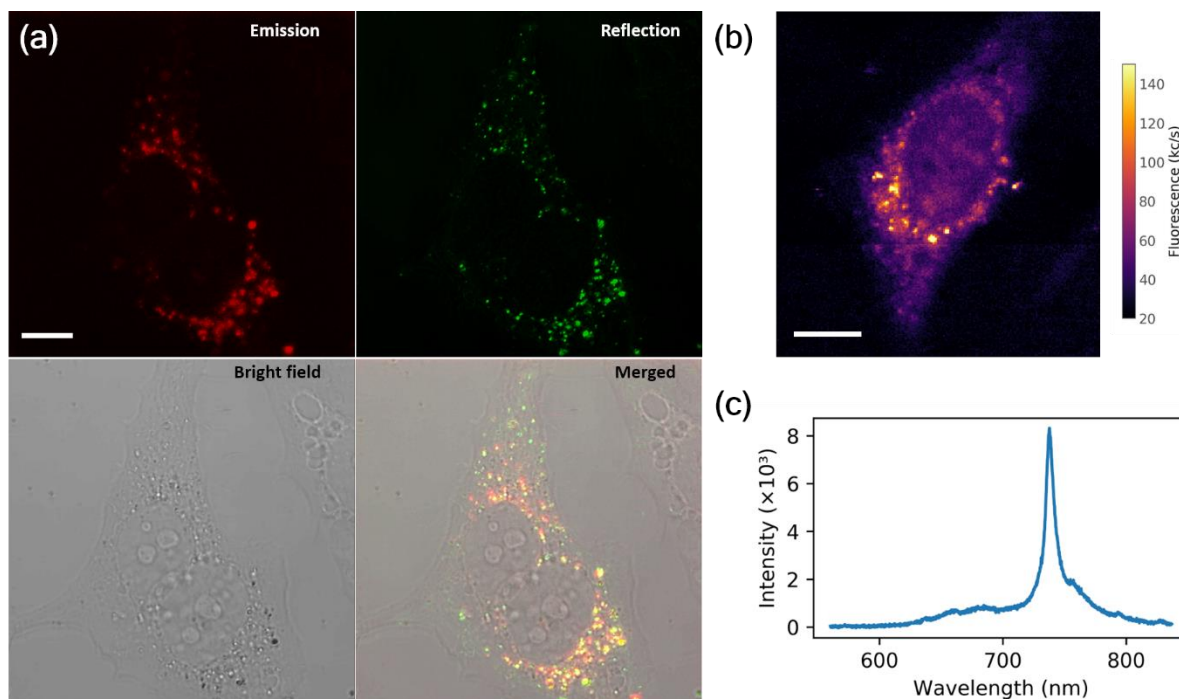

Figure 3. ND$_{SiV}$-polymer for cell imaging. (a) CLSM cell imaging showing efficient cell uptake, emission and reflection channel were applied with very good colocolization (λ_{ex} = 561 nm, λ_{em} = 700 – 758 nm, λ_{re} = 556 – 566 nm, scal bar = 10 µm). (b) The fluorescence cell image by customized scanning confocal microscope (λ_{ex} = 532 nm, λ_{em} = 730 – 770 nm, scal bar = 10 µm). Blank control images for Fig. 3a and 3b was in Fig. S12. (c) The representative SiV fluorescence spectrum measured from an isolated spot on (b), with a clearly sharp zero-phonon-line at 738 nm.

Intracellular tracking of ND$_{SiV}$-polymer. ND$_{SiV}$-polymer as a photostable biomarker was further investigated for cellular tracking on the scanning confocal microscope (see SI for the detailed set-up for 3D-tracking). Note that SiV centers have three dipoles responsible for absorption and emisison. However, their strength is not primarily to afford polarisation

anisotropy.[38-40] Such aniosotropy can lead to fluctuations of fluorescnce intensity in case rotating nanodiamonds are excited with linearly polarised light.

As a preliminary attempt, we have tracked 135 single particle in intervals of 40 s, during a total measurement time of 90 min. Two representative trajectories of two tracked single particles are shown in Fig. 4a-b. The fluorescence intensities of ND$_{SiV}$-polymer during the tracking experiments are given in Fig. 4c. We deduced that in this experiment, the tracked spots contain ~5 SiV$^-$(Tracker 1) and ~4 SiV$^-$ (Tracker 2) by comparing it with the saturated fluorescence intensity (~103 kcounts/s) of a single SiV$^-$ reported in the literature,[41] which was measured with similar experiment configuration (processed under similar fluorescence collection efficiencies). The fluorescence intensities of tracked ND$_{SiV}$-polymer remained relatively stable, with low fluctuations in the fluoresence intensity of Tracker 1. These fluctuations could be attributed to the fast diffusion from the focal point of the objective, or a rotational movement induced by different excitation efficiencies leading to fluorescence intensity changes during tracking. In general, we did not observe significant decrease in the fluorescence intensities indicating that ND$_{SiV}$-polymer allow long-term cellular tracking studies.
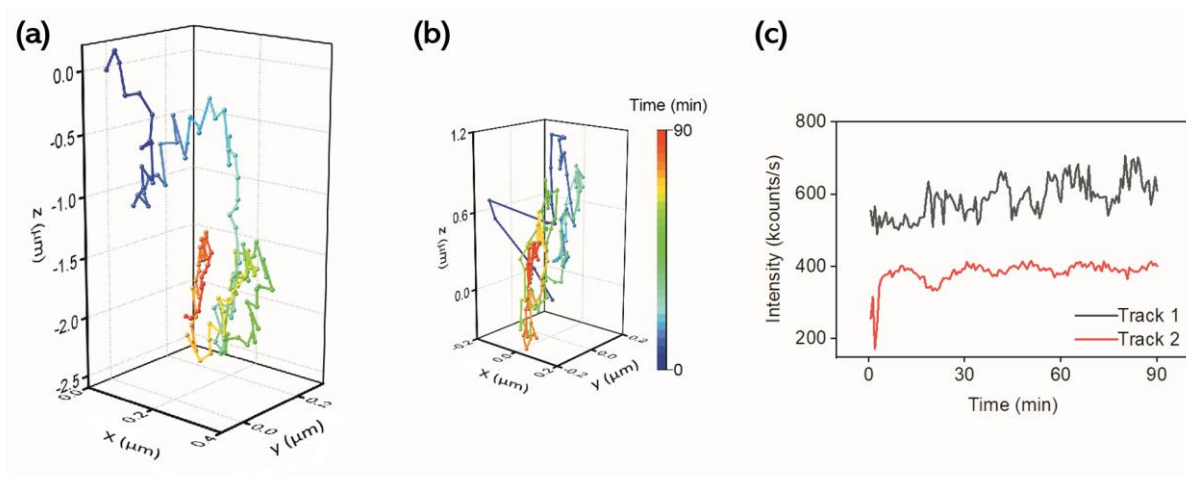

Figure 4. ND$_{SiV}$-polymer for cellular tracking. (a and b) The trajectory of tracked ND-SiV$^-$ spots in intracellular space (a Tracker 1 and b Tracker 2). (c) Fluorescence intensity of the tracked ND-SiV- spots.

Summary and Future Prospective. We have reported an improved preparation method for NDs containg only SiV⁻ color centers without any NV⁻ centers based on the HPHT method. In this way, NIR emitters were obtained with sharp emission peaks that were not affected by the broad NV⁻ emission bands. These new NDs-SiV⁻ emitters coated with a protein-derived biopolymer remained colloidally stable in aqueous solution as well as in cell media. NIR fluoresecence, sharp ZPLs emission, and high fluorescence stability under irradiation were key characteristics of these nanoemitters qualifiying them for living cell imaging and intracellular tracking experiments. Single NDs-SiV⁻ emitters were recorded for the first time inside living cells and we have tracked their movement for up to 90 min.

We believe that NDs-SiV⁻ represent a powerful tool for achieving single particle tracking inside cellular environments with great potential for *in vivo* studies.[42-44] Moreover, NDs-SiV⁻ will offer great opportunities for intracellular real-time temperature sensing due to their ZPLs thermal resonance so that small temperature changes may be detected based on the temprature singature of their intracelluler ZPLs.

ASSOCIATED CONTENT

The Supporting Information is available free of charge on the ACS Publications website at XXX.

AUTHOR INFORMATION

Corresponding Author

*fedor.jelezko@uni-ulm.de *weil@mpip-mainz.mpg.de

Author Contributions

W. Liu and T. Weil initiated the draft. V. N. Agafonov, V. A. Davydov and R. Uzbekov contributed to the HPHT ND-SiV⁻ synthesis and raw material characterization. H. Qi and U. Kaiser contributed to the HRTEM characterization. W. Liu and T. Weil contributed to the ND-SiV⁻ acid treatment, ND_{SiV}-polymer preparation and characterization, bioimaging in CLSM microscopy (Zeiss 710) and cell experiments. Y. Liu and F. Jelezko contributed to the

bioimaging, intracellular tracking and spectral measurements in self-build scanning confocal microscopy and are responsible for the photo physics. T. Lasser contributed writing the manuscript and interpreting experimental data. The manuscript was written through contributions of all authors. All authors have given approval to the final version of the manuscript. ‡W. Liu and Y. Liu contributed equally. W. Liu acknowledges Dr. Todd Zapata (Max Planck Institute for Polymer Research, Germany) and Dr. Qiong Chen（Hunan Normal University, China) for very helpful discussion.

REFERENCE:

1.   Tzeng, Y. K.; Faklaris, O.; Chang, B. M.; Kuo, Y.; Hsu, J. H.; Chang, H. C., Superresolution Imaging of Albumin‐Conjugated Fluorescent Nanodiamonds in Cells by Stimulated Emission Depletion. *Angewandte Chemie International Edition* **2011,** *50* (10), 2262-2265.
2.   Wu, T.-J.; Tzeng, Y.-K.; Chang, W.-W.; Cheng, C.-A.; Kuo, Y.; Chien, C.-H.; Chang, H.-C.; Yu, J., Tracking the engraftment and regenerative capabilities of transplanted lung stem cells using fluorescent nanodiamonds. *Nature Nanotechnology* **2013,** *8*, 682-689.
3.   Ermakova, A.; Pramanik, G.; Cai, J.-M.; Algara-Siller, G.; Kaiser, U.; Weil, T.; Tzeng, Y.-K.; Chang, H.; McGuinness, L.; Plenio, M., Detection of a few metallo-protein molecules using color centers in nanodiamonds. *Nano letters* **2013,** *13* (7), 3305-3309.
4.   Zhang, X.; Hu, W.; Li, J.; Tao, L.; Wei, Y., A comparative study of cellular uptake and cytotoxicity of multi-walled carbon nanotubes, graphene oxide, and nanodiamond. *Toxicology Research* **2012,** *1* (1), 62-68.
5.   Chang, Y.-R.; Lee, H.-Y.; Chen, K.; Chang, C.-C.; Tsai, D.-S.; Fu, C.-C.; Lim, T.-S.; Tzeng, Y.-K.; Fang, C.-Y.; Han, C.-C.; Chang, H.-C.; Fann, W., Mass production and dynamic imaging of fluorescent nanodiamonds. *Nature Nanotechnology* **2008,** *3*, 284-288.
6.   Loubser, J. H. N.; Wyk, J. A. v., Electron spin resonance in the study of diamond. *Reports on Progress in Physics* **1978,** *41* (8), 1201.

7.   Doherty, M. W.; Manson, N. B.; Delaney, P.; Jelezko, F.; Wrachtrup, J.; Hollenberg, L. C., The nitrogen-vacancy colour centre in diamond. *Physics Reports* **2013,** *528* (1), 1-45.

8.   Fu, C.-C.; Lee, H.-Y.; Chen, K.; Lim, T.-S.; Wu, H.-Y.; Lin, P.-K.; Wei, P.-K.; Tsao, P.-H.; Chang, H.-C.; Fann, W., Characterization and application of single fluorescent nanodiamonds as cellular biomarkers. *Proceedings of the National Academy of Sciences* **2007,** *104* (3), 727-732.

9.   Grudinkin, S. A.; Feoktistov, N. A.; Baranov, M. A.; Smirnov, A. N.; Davydov, V. Y.; Golubev, V. G., Low-strain heteroepitaxial nanodiamonds: fabrication and photoluminescence of silicon-vacancy colour centres. *Nanotechnology* **2016,** *27* (39), 395606.

10.   Vlasov, I. I.; Shiryaev, A. A.; Rendler, T.; Steinert, S.; Lee, S.-Y.; Antonov, D.; Vörös, M.; Jelezko, F.; Fisenko, A. V.; Semjonova, L. F.; Biskupek, J.; Kaiser, U.; Lebedev, O. I.; Sildos, I.; Hemmer, P. R.; Konov, V. I.; Gali, A.; Wrachtrup, J., Molecular-sized fluorescent nanodiamonds. *Nature Nanotechnology* **2013,** *9*, 54-58.

11.   Weissleder, R., A clearer vision for in vivo imaging. *Nature Biotechnology* **2001,** *19*, 316-317.

12.   Sajedi, S.; Sabet, H.; Choi Hak, S., Intraoperative biophotonic imaging systems for image-guided interventions. *Nanophotonics* **2018,** *8* (1), 99-116.

13.   Nguyen, C. T.; Evans, R. E.; Sipahigil, A.; Bhaskar, M. K.; Sukachev, D. D.; Agafonov, V. N.; Davydov, V. A.; Kulikova, L. F.; Jelezko, F.; Lukin, M. D., All-optical nanoscale thermometry with silicon-vacancy centers in diamond. *Applied Physics Letters* **2018,** *112* (20), 203102.

14.   Sternschulte, H.; Thonke, K.; Sauer, R.; Münzinger, P. C.; Michler, P., 1.681-eV luminescence center in chemical-vapor-deposited homoepitaxial diamond films. *Physical Review B* **1994,** *50* (19), 14554-14560.

15.   Vlasov, I. I.; Barnard, A. S.; Ralchenko, V. G.; Lebedev, O. I.; Kanzyuba, M. V.; Saveliev, A. V.; Konov, V. I.; Goovaerts, E., Nanodiamond Photoemitters Based on Strong Narrow-Band Luminescence from Silicon-Vacancy Defects. *Advanced Materials* **2009,** *21* (7), 808-812.

16.   Arnault, J. C., *Nanodiamonds: Advanced Material Analysis, Properties and Applications*. Elsevier Science: Amsterdam, 2017.

17.   Alkahtani Masfer, H.; Alghannam, F.; Jiang, L.; Almethen, A.; Rampersaud Arfaan, A.; Brick, R.; Gomes Carmen, L.; Scully Marlan, O.; Hemmer Philip, R., Fluorescent nanodiamonds: past, present, and future. *Nanophotonics* **2018,** *7* (8), 1423-1453.

18.   Shenderova, O. A.; Shames, A. I.; Nunn, N. A.; Torelli, M. D.; Vlasov, I.; Zaitsev, A., Review Article: Synthesis, properties, and applications of fluorescent diamond particles. *Journal of Vacuum Science & Technology B* **2019,** *37* (3), 030802.

19.   Davydov, V. A.; Rakhmanina, A. V.; Agafonov, V.; Narymbetov, B.; Boudou, J. P.; Szwarc, H., Conversion of polycyclic aromatic hydrocarbons to graphite and diamond at high pressures. *Carbon* **2004,** *42* (2), 261-269.

20.   Davydov, V. A.; Rakhmanina, A. V.; Lyapin, S. G.; Ilichev, I. D.; Boldyrev, K. N.; Shiryaev, A. A.; Agafonov, V. N., Production of nano- and microdiamonds with Si-V and N-V luminescent centers at high pressures in systems based on mixtures of hydrocarbon and fluorocarbon compounds. *JETP Letters* **2014,** *99* (10), 585-589.

21.   Davydov, V. A.; Agafonov, V.; Khabashesku, V. N., Comparative Study of Condensation Routes for Formation of Nano- and Microsized Carbon Forms in Hydrocarbon, Fluorocarbon, and Fluoro-Hydrocarbon Systems at High Pressures and Temperatures. *The Journal of Physical Chemistry C* **2016,** *120* (51), 29498-29509.

22.   Choi, S.; Leong, V.; Davydov, V. A.; Agafonov, V. N.; Cheong, M. W. O.; Kalashnikov, D. A.; Krivitsky, L. A., Varying temperature and silicon content in nanodiamond growth: effects on silicon-vacancy centres. *Scientific Reports* **2018,** *8* (1), 3792.

23.   Hsiao, W. W.-W.; Hui, Y. Y.; Tsai, P.-C.; Chang, H.-C., Fluorescent Nanodiamond: A Versatile Tool for Long-Term Cell Tracking, Super-Resolution Imaging, and Nanoscale Temperature Sensing. *Accounts of Chemical Research* **2016,** *49* (3), 400-407.

24.   Hsieh, F.-J.; Chen, Y.-W.; Huang, Y.-K.; Lee, H.-M.; Lin, C.-H.; Chang, H.-C., Correlative Light-Electron Microscopy of Lipid-Encapsulated Fluorescent Nanodiamonds for Nanometric Localization of Cell Surface Antigens. *Analytical Chemistry* **2018,** *90* (3), 1566-1571.

25.   Jung, H.-S.; Cho, K.-J.; Seol, Y.; Takagi, Y.; Dittmore, A.; Roche, P. A.; Neuman, K. C., Polydopamine Encapsulation of Fluorescent Nanodiamonds for Biomedical Applications. *Advanced Functional Materials* **2018,** *28* (33), 1801252.

26.   Wu, Y.; Ermakova, A.; Liu, W.; Pramanik, G.; Vu, T. M.; Kurz, A.; McGuinness, L.; Naydenov, B.; Hafner, S.; Reuter, R.; Wrachtrup, J.; Isoya, J.; Förtsch, C.; Barth, H.; Simmet, T.; Jelezko, F.; Weil, T., Programmable Biopolymers for Advancing Biomedical Applications of Fluorescent Nanodiamonds. *Advanced Functional Materials* **2015,** *25* (42), 6576-6585.

27.   Han, S.; Raabe, M.; Hodgson, L.; Mantell, J.; Verkade, P.; Lasser, T.; Landfester, K.; Weil, T.; Lieberwirth, I., High-Contrast Imaging of Nanodiamonds in Cells by Energy Filtered and Correlative Light-Electron Microscopy: Toward a Quantitative Nanoparticle-Cell Analysis. *Nano Letters* **2019,** *19* (3), 2178-2185.

28.   Davydov, V. A.; Rakhmanina, A. V.; Agafonov, V.; Khabashesku, V. N., On the nature of simultaneous formation of nano- and micron-size diamond fractions under pressure–temperature-induced transformations of binary mixtures of hydrocarbon and fluorocarbon compounds. *Carbon* **2015,** *90*, 231-233.

29.   Nagl, A.; Hemelaar, S. R.; Schirhagl, R., Improving surface and defect center chemistry of fluorescent nanodiamonds for imaging purposes—a review. *Analytical and Bioanalytical Chemistry* **2015,** *407* (25), 7521-7536.

30.   Osswald, S.; Yushin, G.; Mochalin, V.; Kucheyev, S. O.; Gogotsi, Y., Control of sp2/sp3 Carbon Ratio and Surface Chemistry of Nanodiamond Powders by Selective Oxidation in Air. *Journal of the American Chemical Society* **2006,** *128* (35), 11635-11642.

31.   Koynov, K.; Butt, H.-J., Fluorescence correlation spectroscopy in colloid and interface science. *Current Opinion in Colloid & Interface Science* **2012,** *17* (6), 377-387.

32.   Schaeffel, D.; Yordanov, S.; Staff, R. H.; Kreyes, A.; Zhao, Y.; Schmidt, M.; Landfester, K.; Hofkens, J.; Butt, H.-J.; Crespy, D.; Koynov, K., Fluorescence Correlation Spectroscopy in Dilute Polymer Solutions: Effects of Molar Mass Dispersity and the Type of Fluorescent Labeling. *ACS Macro Letters* **2015,** *4* (2), 171-176.

33.   Merson, T. D.; Castelletto, S.; Aharonovich, I.; Turbic, A.; Kilpatrick, T. J.; Turnley, A. M., Nanodiamonds with silicon vacancy defects for nontoxic photostable fluorescent labeling of neural precursor cells. *Optics Letters* **2013,** *38* (20), 4170-4173.

34.   Chunlang, W.; Christian, K.; Harald, W.; Bernd, B., Single photon emission from SiV centres in diamond produced by ion implantation. *Journal of Physics B: Atomic, Molecular and Optical Physics* **2006,** *39* (1), 37-41.

35.   Wu, Y.; Eisele, K.; Doroshenko, M.; Algara-Siller, G.; Kaiser, U.; Koynov, K.; Weil, T., A Quantum Dot Photoswitch for DNA Detection, Gene Transfection, and Live-Cell Imaging. *Small* **2012,** *8* (22), 3465-3475.

36.   Zhang, T.; Neumann, A.; Lindlau, J.; Wu, Y.; Pramanik, G.; Naydenov, B.; Jelezko, F.; Schüder, F.; Huber, S.; Huber, M.; Stehr, F.; Högele, A.; Weil, T.; Liedl, T., DNA-Based Self-Assembly of Fluorescent Nanodiamonds. *Journal of the American Chemical Society* **2015,** *137* (31), 9776-9779.

37.   Neu, E.; Agio, M.; Becher, C., Photophysics of single silicon vacancy centers in diamond: implications for single photon emission. *Optics Express* **2012,** *20* (18), 19956-19971.

38.   Hepp, C.; Müller, T.; Waselowski, V.; Becker, J. N.; Pingault, B.; Sternschulte, H.; Steinmüller-Nethl, D.; Gali, A.; Maze, J. R.; Atatüre, M.; Becher, C., Electronic Structure of the Silicon Vacancy Color Center in Diamond. *Physical Review Letters* **2014,** *112* (3), 036405.

39.   Rogers, L. J.; Jahnke, K. D.; Doherty, M. W.; Dietrich, A.; McGuinness, L. P.; Müller, C.; Teraji, T.; Sumiya, H.; Isoya, J.; Manson, N. B.; Jelezko, F., Electronic structure of the negatively charged silicon-vacancy center in diamond. *Physical Review B* **2014,** *89* (23), 235101.

40.   Liu, Y.; Chen, G.; Rong, Y.; McGuinness, L. P.; Jelezko, F.; Tamura, S.; Tanii, T.; Teraji, T.; Onoda, S.; Ohshima, T.; Isoya, J.; Shinada, T.; Wu, E.; Zeng, H., Fluorescence Polarization Switching from a Single Silicon Vacancy Colour Centre in Diamond. *Scientific Reports* **2015,** *5*, 12244.

41.   Liu, Y.; Siyushev, P.; Rong, Y.; Wu, B.; McGuinness, L. P.; Jelezko, F.; Tamura, S.; Tanii, T.; Teraji, T.; Onoda, S.; Ohshima, T.; Isoya, J.; Shinada, T.; Zeng, H.; Wu, E., Investigation of the silicon vacancy color center for quantum key distribution. *Optics Express* **2015,** *23* (26), 32961-32967.

42.   McGuinness, L. P.; Yan, Y.; Stacey, A.; Simpson, D. A.; Hall, L. T.; Maclaurin, D.; Prawer, S.; Mulvaney, P.; Wrachtrup, J.; Caruso, F.; Scholten, R. E.; Hollenberg, L. C. L., Quantum measurement and orientation tracking of fluorescent nanodiamonds inside living cells. *Nature Nanotechnology* **2011,** *6*, 358-363.

43.   Haziza, S.; Mohan, N.; Loe-Mie, Y.; Lepagnol-Bestel, A.-M.; Massou, S.; Adam, M.-P.; Le, X. L.; Viard, J.; Plancon, C.; Daudin, R.; Koebel, P.; Dorard, E.; Rose, C.; Hsieh, F.-J.; Wu, C.-C.; Potier, B.; Herault, Y.; Sala, C.; Corvin, A.; Allinquant, B.; Chang, H.-C.; Treussart, F.; Simonneau, M., Fluorescent nanodiamond tracking reveals intraneuronal transport abnormalities induced by brain-disease-related genetic risk factors. *Nature Nanotechnology* **2016,** *12*, 322-328.

44.   Wang, F.; Wen, S.; He, H.; Wang, B.; Zhou, Z.; Shimoni, O.; Jin, D., Microscopic inspection and tracking of single upconversion nanoparticles in living cells. *Light: Science &Amp; Applications* **2018,** *7*, 18007.